Dynamic Viscosity of Some Lubricants in Terms of Local Nano-Void Fraction

F. Sahin-Dinc*

Machinery Department, Machinery and Metal Technologies, Surmene Abdullah Kanca Vocational School, Karadeniz Technical University, 61530, Camburnu, Surmene, Trabzon, Turkey

Received: 21.01.2023 & Accepted: 09.08.2023

Doi: 10.12693/APhysPolA.144.180 *e-mail: fatmadinc@ktu.edu.tr

In the current study, the dynamic viscosity has been established by the preceding viscosity correlation equation in terms of thermo-occupancy function, $Y_h = Y_h(h,T)$, for three types of chemically different pure substances between 283.15–398.15 K and up to 100 MPa. The thermo-occupancy function, $Y_h = Y_h(h,T)$, comprises temperature T and hole (nano-void) fraction $h = h(P,T)$ estimated by the Simha–Somcynsky equation of state through the published density data. The density fitting results were found by this report to be from 0.026 to 0.051%. The predictive dynamic viscosity of dialkyl carbonates, ethylene glycol dimethyl ethers, and di(2-ethylhexyl) sebacate was obtained with an overall uncertainty of 0.29%, 0.40%, and 0.38%, respectively. The effects of the optimized volumetric and rheological parameters on the compounds' molecular structure and architecture were investigated. The increase in fraction h with an increasing temperature suggests a decrease in the rate of change in dynamic viscosity (viscoholibility) of the samples over a computed hole fraction range.

topics: dynamic viscosity, dialkyl carbonates, glymes, di(2-ethylhexyl) sebacate

1. Introduction

There are quick advances in most aspects of industrial applications, from personal care to food and from marine to aerospace. These applications promoted the interest in finding new environmentally benign chemical products and safe processes. Among them, ethylene glycol dimethyl ethers (glymes) and dialkyl carbonates (DACs) have attracted widespread attention as working fluids, lubricants, and solvents over the last several decades. Because of their outstanding properties, like low bioaccumulation, negligible vapor pressure, low toxicity, low viscosity, heat absorbing capability, nonflammability, high chemical stability, high thermal stability, low melting point, excellent solubility, excellent blending property [1], they are the potential contenders to supersede many hazardous chemicals in various applications. Glymes and DACs are treated as green absorbent fluids in the application of absorption cycles for upgrading waste heat and refrigeration cycles. For this purpose, they are used in HFCs (hydrofluorocarbons) [2, 3] instead of ozone-depleting substances, CFCs (chlorofluorocarbons) refrigerants, or classical ammonia+water/water+lithium bromide mixtures systems [4]. The latter have some drawbacks and some toxic effects at high-temperature applications where glymes and organic carbonates, DACs, can be used due to their thermal stability. In order to inhibit the wear and failure of compressor elements of air conditioning systems and refrigerations, both glymes and DACs are utilized in elastohydrodynamic lubrication (EHL) for HFC refrigerants [2, 3]. Due to the increased depletion of fossil fuels, destruction of the stratospheric ozone layer, and the tremendous contribution of CFCs to the greenhouse effect, these important linear carbonates are promoted as the alternatives to diesel/gasoline fuels or additives for conventional hydrocarbon fuels [1, 5–9]. DACs have outstanding blending properties and oxygen content as well as low bioaccumulation properties, and as a result, they have higher biodegradability and are environmentally friendly. By reducing the vapor pressure of fuels due to their own low vapor pressure, DACs curtail the emission of CO_2 together with particulates/pollutants from diesel engines to the atmosphere and, in this sense, improve combustion [1, 6, 8, 9]. Besides being used as fuel constituents and absorbents, and

being excellent CO_2-expanded bio-sourced solvents and inviscid materials, DACs are also introduced as potential electrolytes in order to improve the conductivity of the electrolyte for lithium ion (Li-ion) cells in the energy storage from solar and wind energy sources and in the rechargeable battery technology for sophisticated electric vehicles [9–11]. They are also used for the synthesis of new chemicals, for example, isocyanates and polycarbonates, a type of engineering plastics, as well as for the manufacture of agrochemicals (pesticides), fertilizers, antioxidants, adhesives, pharmaceutical products, dyestuffs, and so on [6, 9].

Besides the use of glymes and DACs for high-pressure viscosity processes such as enhanced oil recovery, polymer processing, and lubrications, di(2-ethylhexyl) sebacate (DEHS) emerges as a contender for many lubricant applications [12–14]. For example, it enhances the mobility at lower temperatures in gearbox assemblies in which pressure is brought in from the engine to a driving axle, like in compressors, pumps, and so on. Bis(2-ethylhexyl) sebacate (BIS) is ideally suited as a pressure transmitting fluid (PTF) in multiple industries, including civil aviation [15], automotive, military [16], and food industry during the process of freezing and sterilization [17]. DEHS is used to transmit pressure in high-pressure processes involving hydraulic pressure balances [16], pressure measuring instruments (like piston gauges) [16, 18], hydraulically operated devices [19], and other pressure transmission applications. These applications include the working principles and operation processes of gears, final drives processing equipment, piston pumps, piston gauges, compressors, and combustion engines [12, 20]. In recent years, pure DEHS, due to its low compressibility, has become an alternative for a high-viscosity reference lubricant in high-pressure calibration processes for verification and optimization of measurement standards as well as validation of the measuring apparatus [12, 21, 22]. DEHS is mainly used as a plasticizer found in toys and childcare items [23]. It has already found use in our daily life as a personal care product, an automotive care product, an electronic product, and a food product [23]. More precisely, in the food industry, it is used in food control substances as an indirect additive and a food packing film [23]. Because of its relatively low boiling point, low vapor pressure, and low toxicity, it is utilized to produce nontoxic aerosols, including fragrances and fresheners [23].

Improving the performance of the aforementioned liquids, processes, and applications in comprehensive designing, manufacturing, fabrication, development, analysis, and characterization of high-pressure instruments requires an understanding of the interrelations between the microstructure and mechanical characterizations of these fluids under high pressure. For these practical concerns, it is of vital importance to have knowledge of several thermodynamic, thermophysical, and transport properties, specifically viscosity. Data for lubricant film thickness calculations, simple EHL models, and proximity equations utilized to estimate the coefficient of friction between liquid film-lubricated interfaces necessitate the rheology of the lubricant, namely the temperature- and pressure-dependent viscosity [22]. Inaccuracy in any of the mentioned computations can produce wear and fatigue mechanisms, power losses in rolling bearings and gears, etc. [22]. Viscosity relationship with some measurable volumetric properties such as density or its reciprocal value, so-called specific volume, also occupies a prominent place. The specific volume data along various isotherms and isobars give a way to produce free volume fraction by means of the Simha–Somcynsky equation of state (SS-EoS) and is required as an input to determine and model the viscosity (see [24, 25] and the references given therein).

Here, the author presents new inputs to theoretical dynamic viscosity in order to reduce the unmeasured region for two dialkyl carbonates (DACs), two ethylene glycol dimethyl ethers, and a di(2-ethylhexyl) sebacate (DEHS) from 283.15 to 398.15 K up to 100 MPa. The results obtained by the dynamic viscosity model established in earlier studies [24, 25] are also compared with observations from the literature to assure theoretical reliability. Subsequently, in this work, the author provides an overview regarding the attempt to interpret the volumetric and rheological results in terms of hole fraction.

2. Theory

2.1. The Simha–Somcynsky equation of state (SS-EoS) in connection with zero-shear viscosity correlation equation

In Eyring significant structure theory (ESS), the viscosity of the solid part of liquid [26, 27] is determined to be

$$\eta_{sp} = (1 - h)\,\eta_s, \tag{1}$$

where η_{sp} and η_s correspond to the solid-part and solid-like viscosities, respectively. The temperature- and pressure-dependent hole fraction parameter is denoted by $h = h(P, T)$.

The solid-like viscosity of a liquid η_s, in (1), can be replaced with the Newtonian viscosity $\eta_N = \frac{3\sqrt{2}s}{q_z h}\frac{k_\mathrm{B}T}{\upsilon\, k'}$, which is described as the dynamic viscosity comprising the Eyring strain rate[28]. Thus,

$$\eta_{sp} = (1 - h)\,\frac{3\sqrt{2}\,s}{q_z h}\,\frac{k_\mathrm{B}T}{\upsilon\, k'}, \tag{2}$$

in which k_B, s, and υ are referred to as the Boltzmann constant, the segment number, and the segmental volume, respectively. The total number of possible ligands available among s segments in a

lattice of the ligancy z is q_z which is fixed at $z = 12$. The Eying jumping frequency is represented by k' and defined by

$$k' = \kappa \frac{k_{\mathrm{B}}T}{h_{\mathrm{p}}} \frac{Z^*}{Z} \exp\left(-\frac{E_a}{k_{\mathrm{B}}T}\right), \tag{3}$$

where κ and h_{p} denote the transmission coefficient and the Planck constant, respectively. The fraction Z^*/Z for a molecule characterizes the quotient of the partition functions being in the flow-activated condition to that at equilibrium and is given as [28–31]

$$\frac{Z}{Z^*} = \frac{\exp\left(-\dfrac{h_{\mathrm{p}}v}{2k_{\mathrm{B}}T}\right)}{1 - \exp\left(-\dfrac{h_{\mathrm{p}}v}{k_{\mathrm{B}}T}\right)}. \tag{4}$$

In (4), it is assumed that during flow, one of the vibrational modes in an equilibrium condition has been transformed into a translational state in an activated mode.

In (3), the flow-activation energy of a segment needed for jumping is E_a of the form

$$E_a = \frac{a'}{2} \frac{(1-h)}{h} q_z \Phi, \tag{5}$$

where Φ is referred to as the Lennard–Jones potential energy arising from the segment–segment interaction, and a' is the activation energy proportionality constant.

Substituting (3), (4), and (5) in (2) and taking the logarithm of both sides [24, 25, 29], one obtains

$$\ln\left(\frac{h}{1-h} \frac{1 - \mathrm{e}^{-h_{\mathrm{p}}v/(k_{\mathrm{B}}T)}}{\mathrm{e}^{-h_{\mathrm{p}}v/(2k_{\mathrm{B}}T)}} v\eta_{sp}\right) = \ln(\eta^*) + \alpha \frac{(1-h)}{h} \frac{1}{T}. \tag{6}$$

The right-hand side of (6) corresponds to the logarithm of zero-shear viscosity, $\ln(\eta_0)$, i.e.,

$$\ln(\eta_0) = \ln(\eta^*) + \alpha \frac{(1-h)}{h} \frac{1}{T}, \tag{7}$$

where η^* stands for the viscosity extrapolation at the maximum free volume fraction at the highest temperature and lowest pressure. The measure of activation energy is α. These parameters are ascertained to be

$$\eta^* = \frac{3s\sqrt{2}\, N_{\mathrm{A}} h_{\mathrm{p}}}{q_z \kappa} \quad \text{and} \quad \alpha = a' \frac{q_z \Phi}{2k_{\mathrm{B}}}. \tag{8}$$

In (7), the quotient of the fraction $\frac{1-h}{h}$ to absolute temperature (T) is designated as the *thermo-occupancy* function and represented by [32–35]

$$Y_h = \frac{1-h}{h\,T}. \tag{9}$$

The thermo-occupancy function, Y_h, bridges the equilibrium and transport properties of fluids through the thermophysical characteristics of materials, specifically, hole fraction $h = h(P,T)$ attained from the equilibrium condition in Simha–Somcynsky equation of state (SS-EoS). The form of SS-EoS is the following

$$\frac{\tilde{P}\tilde{V}}{\tilde{T}} = (1-\beta)^{-1} + \frac{2y}{\tilde{T}} (y\tilde{V})^{-2} \left[A(y\tilde{V})^{-2} - B\right]$$

$$\left[\frac{s-1}{s} + \frac{\ln(1-y)}{y}\right] \frac{s}{3c} = \left(\beta - \frac{1}{3}\right)\left(1-\beta\right)^{-1} + \frac{y}{6\tilde{T}} (y\tilde{V})^{-2} \left[2A - 3B(y\tilde{V})^{-2}\right], \tag{10}$$

where the quantities with tilde $\tilde{P}$, $\tilde{V}$, and $\tilde{T}$ signify the reduced pressure, volume, and temperature parameters. They are respectively characterized using three scaling parameters, P^*, V^*, and T^*, appearing as $\tilde{P} = P(P^*)^{-1}$, $\tilde{V} = V(V^*)^{-1}$, and $\tilde{T} = T(T^*)^{-1}$. The detailed description about these parameters is given in Appendix A. The occupied site fraction in terms of hole fraction is $y = 1 - h$. The structural flexibility quantity is $3c/s$, where s corresponds to the chain length and $3c$ is referred to as the number of external degrees of freedom per molecule.

The "viscoholibility" notion is a portmanteau word that originated in concepts of viscosity and hole fraction, indicates the rate of change in viscosity of a sample over a given temperature range, and is derived from the differentiation of (7) with respect to hole fraction at a constant absolute temperature [32–35]

$$\left.\frac{\partial \ln(\eta_0)}{\partial h}\right|_T = -\frac{\alpha}{h^2 T}. \tag{11}$$

3. Calculations and discussion

3.1. The SS theory analysis of PVT data

The volumetric data of two dialkyl carbonates and two polyethers (two glymes) examined in this work were provided by Comunas et al. [3] for the temperature range 283.15–353.15 K and for the range of pressures from 0.1 to 60 MPa, as compiled in Table I. The density measurement in terms of pressure and temperature is performed with an Anton Paar DMA 60/512P vibrating tube densimeter. The density observations of Paredes et al. [12] for di(2-ethylhexyl) sebacate (DEHS) are determined with the aid of a vibrating tube densimeter at temperatures from 298.15 to 398.15 K and pressures from 0.1 to 60 MPa. Technical details are provided in [3, 12].

The density data of three dissimilar chemical classes were investigated in this study. The sample liquid constituents tested are dialkyl carbonates (DACs): dimethyl carbonate (carbonic acid dimethyl ester) (DMC) and diethyl carbonate (carbonic acid diethyl ester) (DEC) [$(CH_3–(CH_2)_{n-1}–O)_2CO$ with $n = 1$, 2, respectively]; two polyethers (two alkylene glycol dialkyl ethers) [$CH_3O–((CH_2)_2O)_n–CH_3$ with $n = 3$, 4]: triethylene glycol dimethyl ether (triglyme) (TriEGDME)

TABLE I

Characteristics of materials.

Materials	Hill (emprical) formula	MW [g/mol]	Temp. range[a] [K]	Pressure range[b] [MPa]
DMC	$C_3H_6O_3$	90.08	283.15–353.15	0.1–100
DEC	$C_5H_{10}O_3$	118.13	283.15–353.15	0.1–100
TriEGDME	$C_8H_{18}O_4$	178.222	283.15–353.15	0.1–100
TEGDME	$C_{10}H_{22}O_5$	222.281	323.15–353.15	0.1–100
DEHS	$C_{26}H_{50}O_4$	426.682	298.15–398.15	0.1–60

[a]Temperature range used for PVT and viscosity data

[b]Pressure range used for PVT and viscosity data

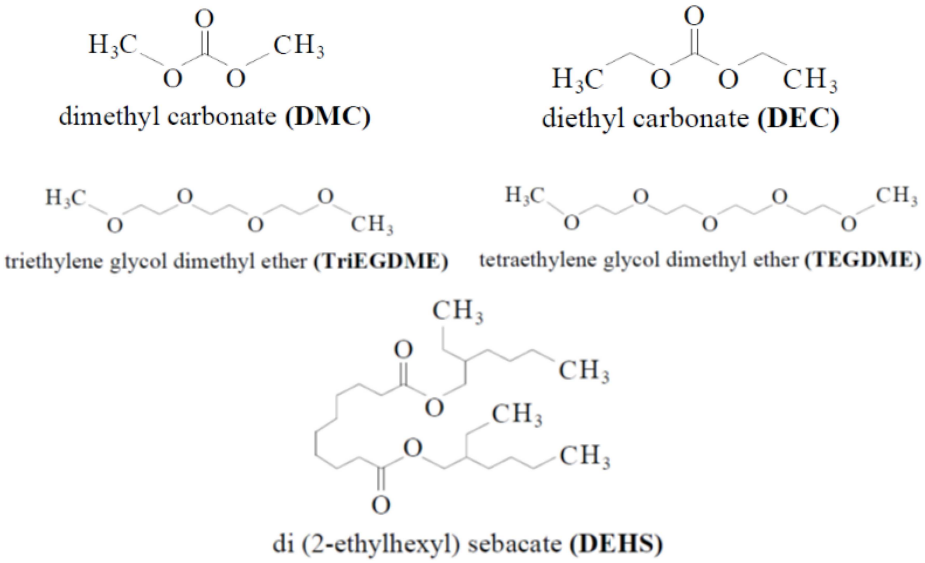

Fig. 1. Structural formulae of samples.

$[CH_3OCH_2(CH_2OCH_2)_2CH_2OCH_3]$ and tetraethylene glycol dimethyl ether (tetraglyme) (TEGDME) $[CH_3OCH_2(CH_2OCH_2)_3CH_2OCH_3]$; and a diester: di(2-ethylhexyl) sebacate (DEHS) or bis(2-ethylhexyl) sebacate (BIS) (visualized in Fig. 1).

The SS-EoS given in (1) as PVT inputs to the dynamic viscosity equation yields the characteristic parameters V^*, T^*, P^*, the structural flexibility quantity $3c/s$, and Lennard–Jones interaction measures (v^* and ε^*) together with hole fraction $h = h(\tilde{P}, \tilde{T})$ to estimate the viscosity and its derivation. The chain length s corresponds to the sum of carbon and oxygen numbers, while the evaluation parameter c is taken as a dispensable quantity in structural flexibility parameter $3c/s$.

The N number of equations incorporating the reducing parameters V^* and T^* are obtained by projecting the N number of PVT observations on the theory for the simultaneous analysis of the complete data set. The equations also comprise P^* in terms of V^* and T^* for the settled c and s values. Subsequently, each equation expands to the first power, evaluated for the unspecified V^* and T^* parameters by employing the Newton–Raphson method in the Mathematica program [36]. The ultimate best-fit parameters, together with the computed V^* and T^*, for the tested chemicals were obtained and revealed in Table II. Further details can be found in Appendix A. The hole fraction, $h(P, T)$, was also evaluated in order to use it to predict the dynamic viscosity and its parameters discussed in Sect. 3.2. The minimum relative mean absolute percentage error (rMAPE) between theoretical and reported specific volume determined by fitting (10) to PVT literature data of five materials varies from 0.026 to 0.051. The SS-EoS fit result for rMAPE is determined by

$$\Delta V\,[\%] = \frac{100}{N}\sum\nolimits_i \frac{\left|V_i^{\exp} - V_i^{\mathrm{calc}}\right|}{V_i^{\exp}}. \tag{12}$$

Lennard–Jones average energetic, $\langle\varepsilon^*\rangle$, and volumetric, $\langle v^*\rangle$, quantities are evaluated and recorded in Table II. The $\langle\varepsilon^*\rangle$ values range from 133.362 to 156.219 for the studied species. The magnitude of the mean characteristic repulsive molar volume $\langle v^*\rangle$, which has opposite trends to the mean characteristic attractive interaction energy $\langle\varepsilon^*\rangle$, ranges from 12.71 to 15.25 for the constituents under investigation. The ester and the ethers (glymes) with longer chained structures are denser and have increasing effects in $\langle\varepsilon^*\rangle$ compared to short-chain

TABLE II

Physicochemical characteristic parameters based on the PVT results.

Parameter	DMC	DEC	TriEGDME	TEGDME	DEHS
m_0 ($\times 10^3$) [kg]	15.01	14.77	14.85	14.82	14.22
s	6	8	12	15	30
c	0.9	1.06	1.78	2.17	2.72
$\langle -\Phi/k \rangle^*$ [K]	198.55	191.11	220.36	223.76	199.80
V^* ($\times 10^3$) [m^3/kg]	0.84645	0.93945	0.95289	0.93635	1.07255
T^* [K]	9549.01	10316.7	10544.2	10942.5	15479.3
P^* [MPa]	937.125	819.271	918.836	948.555	764.928
$\langle v^* \rangle$ ($\times 10^6$) [m^3/mol]	12.71	13.87	14.15	13.88	15.25
$\langle \varepsilon^* \rangle$ [K]	138.615	133.362	153.841	156.219	139.417
ΔV [%]	0.026	0.038	0.028	0.027	0.051
$\max \Delta V$ [%]	0.091	0.38	0.064	0.065	0.136

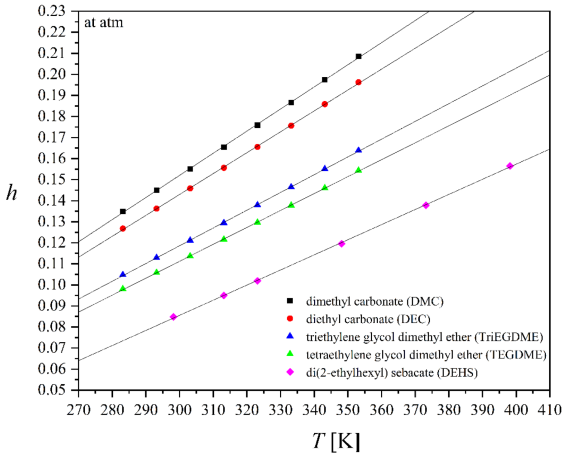

Fig. 2. Variation in h with T at atmospheric pressure for each sample.

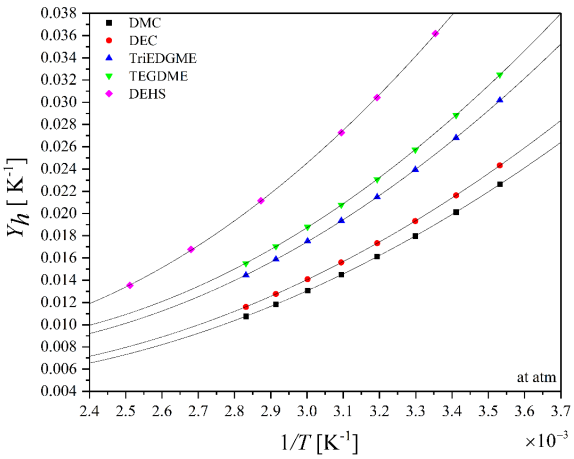

Fig. 3. Variation in Y_h with T^{-1} at atmospheric pressure for each sample.

carbonates, i.e., DMC and DEC. In addition, the two glymes show the highest $\langle \varepsilon^* \rangle$ of all because of the strong dipole–dipole interactions induced by the polar ether groups (CH_3–O–CH_2–CH_3). When comparing the outcomes acquired for glymes with those of the corresponding alkanes examined in the previous study [25], the molar masses of the alkanes are scarcely lower than the corresponding glyme values. Further, the density of the glymes [3] is noticeably higher than that of alkanes [37, 38]. Therefore, the characteristic molar volume of alkanes, $\langle v^* \rangle$, is appreciably higher, but $\langle \varepsilon^* \rangle$ is lower than the glycol ethers studied [3] since $\langle v^* \rangle$ and $\langle \varepsilon^* \rangle$ are inversely related to each other.

The molecular structure influence on nano-void fraction for the tested materials at each T and 1 atm computed from (10) is delineated in Fig. 2. The colored geometrical shapes designate the theoretical h values, and the solid lines represent the best-fit lines through each evaluation set. The h values increase with temperature, and more free volume is produced since the molecules acquire more kinetic energy and thus move apart from each other. In the figure, while DMC (carbonic acid dimethyl ester) has the highest hole fraction, the sample with the lowest hole fraction is DEHS.

The thermo-occupancy function, Y_h, for which transport properties are specified, was obtained from the SS-EoS model fit. The variations of Y_h of samples with the reciprocal temperature at ambient pressure are depicted in Fig. 3. The fits are designated as colored geometrical shapes together with the curves for eye guiding. The magnitude of Y_h ascends as temperature dwindles for each material in Fig. 3. At a fixed Y_h value, DEHS has the greatest transport stability of all samples in terms of Y_h. The two glycol ethers (TEGDME and TriEGDME) have greater transport stability than dialkyl carbonates (DEC and DMC). DEC (carbonic acid diethyl ester) has greater transport stability than DMC and TEGDME than TriEGDME. Subsequently, as the increased number of CH_2 (methylene) groups are available from DMC to DEC and from TriEGDME to TEGDME, the stability goes up.

The extrapolated values at 0°C for h and Y_h in Figs. 2 and 3, respectively, are compiled for each

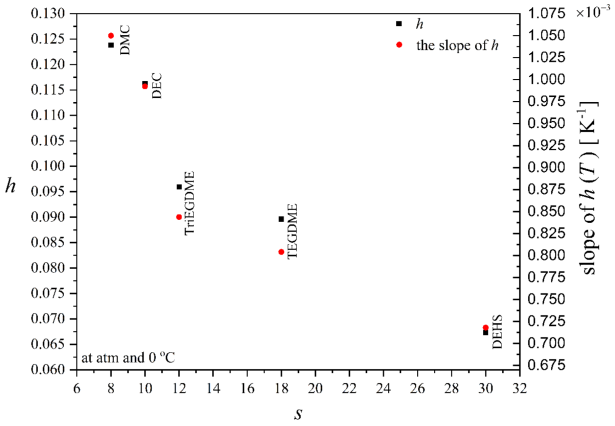

Fig. 4. A graph of the variation of h (at 1 atm and 0°C) and the slope of the lines in Fig. 2 at 1 atm with respect to s.

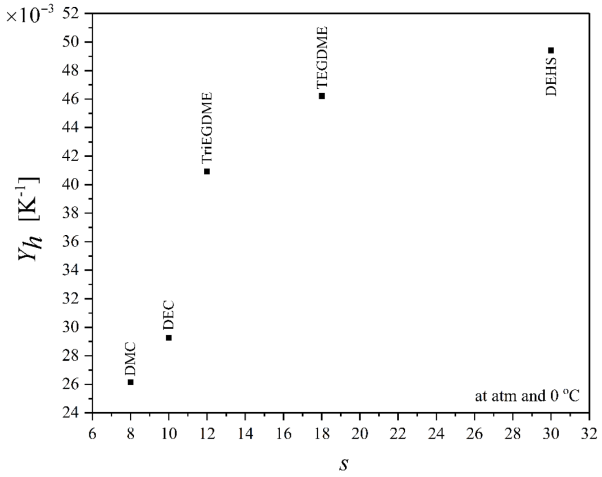

Fig. 5. Variation in Y_h with s at atmospheric pressure and 0°C for each sample.

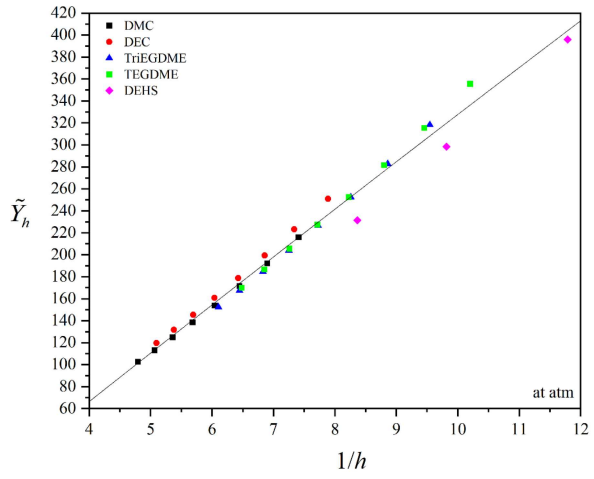

Fig. 6. Variation in $\tilde{Y}_h$ with $1/h$ at atmospheric pressure and 0°C for each sample.

TABLE III

The slope of h and the values extrapolated at 0°C for h and Y_h at 1 atm for the tested compounds.

Materials	h at 0°C	Slope of $h(T)$ ($\times 10^{-3}$) [K^{-1}]	Y_h ($\times 10^{-3}$) [K^{-1}] at 0°C
DMC	0.124	1.05	26.15
DEC	0.116	0.994	29.27
TriEGDME	0.096	0.844	40.94
TEGDME	0.090	0.804	46.22
DEHS	0.067	0.718	49.42

liquid in Table III. The slopes of the dynamic viscosity fitting lines in Fig. 2 are also included in Table III. For the studied two dialkyl carbonates, polyethers and the ester, the computed h values vary with the decreasing values from DMC to DEC and from TriEGDME to TEGDME and DEHS. As the chain length increases and the molecule becomes more compact, the fractional hole fraction (h) decreases. The thermooccupancy functional behavior of the materials is the opposite of the h results, as evident in Table III.

The slope of the lines (temperature coefficient of hole fraction) in Fig. 2 also demonstrates the same reduction pattern with hole fraction effects while going from short to long-chain materials. One more evaluation inferred from Table III is that the diester (bis(2-ethylhexyl) sebacate), at similar temperature and pressure ranges with dialkyl carbonates and glycol ethers, has less free volume as a vacancy defect and hence more viscous behaviour compared to the organic carbonates and glymes.

Figure 4 visualizes the results in Table III as a graph of the variation of hole fraction at 1 atm and 0°C along with the slope of the lines in Fig. 2 with segment number s. Both h and the slope of h descend with a growth in the chain length of the sample in Fig. 4. It means that while the chain length and the number of CH_2 groups (that gives increased stability to the molecule) increase, both the fraction h and the slope of it decrease. From the figure, it is obvious that both h and the slope of h values are higher for dialkyl carbonates than for polyalkylene glycol dimethyl ethers and the ester with the corresponding segment number, since the latter have more stable structures.

The changes in the magnitude of Y_h regarding segment number, s, are delineated in Fig. 5 for the individual materials. It is visible in the figure that Y_h values get higher with the increasing s for all chemical groups. The ester and polyethers (glymes) have higher transportation stability compared to dialkyl carbonates for the corresponding s number. From dialkyl carbonates to ethylene glycol dimethyl ethers and ester, stability increases as the molecules are tightly packed due to the increased number

TABLE IV

Hole fraction correlation to viscosity (see (7)) together with data fit statistics.

Materials	$\ln(\eta^*)$	α	a' $(\times 10^{-2})$	κ	$\Delta\eta$ [%]	R^2
DMC	−18.90	44.85	0.75	0.027	0.28	0.99999
DEC	−18.71	44.70	0.59	0.022	0.30	0.99999
TriEGDME	−18.51	55.98	0.42	0.018	0.37	0.99998
TEGDME	−18.34	61.26	0.37	0.016	0.42	0.99997
DEHS	−18.27	83.43	0.28	0.014	0.38	0.99998

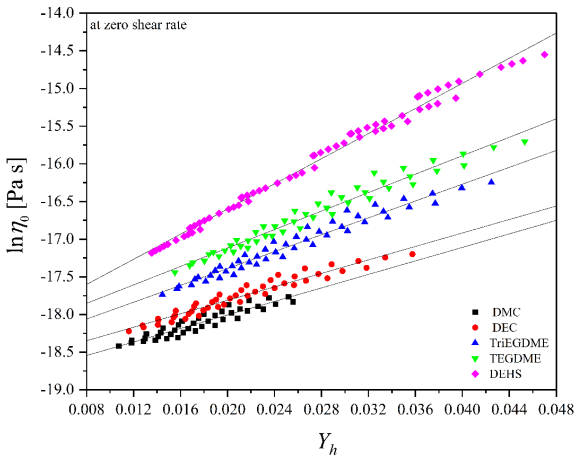

Fig. 7. Correlations between $\ln(\eta_0)$ and Y_h by means of (7) and (9) for each sample.

of CH_2 (methylene) or C_2H_4 (ethylene) groups. DEHS exhibits the highest transportation stability, while dialkyl carbonates represent the lowest one. The order of the computed values of Y_h at 1 atm and 0°C for both the dialkyl carbonates and glymes along with ester is as follows: DEHS > TEGDME > TriEGDME > DEC > DMC.

Figure 6 illustrates the estimated hole fraction dependence of the thermo-occupancy function in a reduced temperature, $\tilde{Y}_h(h, \tilde{T})$, versus the reciprocal value of h, at ambient pressure. The universal curve represents the best-fit line through the predicted points for all the samples researched. The curve indicates that the $\tilde{Y}_h$ function of occupancy typically increases with decreasing h as a measure of configurational stability. The more thermodynamic transportation stability in the structure is represented by $\tilde{Y}_h$ and ultimately indicates the more viscous effect.

3.2. Fitting the zero-shear viscosity model

Section 3.1, titled "The SS theory analysis of PVT data," is about the prediction of the SS theory parameters alongside the hole fraction for the corresponding pressure and temperature. In the present section, using the hole fraction results, we predict the viscosity of the materials under study via the earlier reported zero-shear viscosity model. More precisely, the discussion is about the viscosity prediction with the fitting parameters and its relation to the vacancy fraction as a particular type of free volume fraction.

The database regarding viscosity is acquired from the open literature [3, 12]. Temperature and pressure range for viscosity is similar to PVT data given in Table I: $283.15 \leq T \leq 353.15$ K and $0.1 \leq P \leq 100$ MPa for two dialkyl carbonates and two polyethers (glymes). The viscosity of these samples at atmospheric pressure is determined with a Ubbelohde-type glass capillary-tube viscometer. For the high-pressure viscosity measurement, a falling body viscometer is used. For bis(2-ethylhexyl) sebacate (BIS), the viscosity at atmospheric pressure was measured with a rotational automated viscometer Anton Paar Stabinger SVM 3000. The viscosity measurements at high pressure were performed in a rolling-ball viscometer in the range of 298.15 to 398.15 K and 0.1 to 60 MPa. The technical details and the procedure of the measurements can be found in [3, 12].

The measured viscosity observations have been fitted in terms of thermo-occupancy function, Y_h, through (7). The predicted thermo-occupancy function, Y_h, incorporating temperature and the hole fraction, allows estimating the viscosity in (7). The regression quantities produced by (7) and (8), i.e., κ and $\ln(\eta^*)$ together with α and a', are compiled in Table IV. The data statistics, namely the coefficient of determination, R^2, and the relative mean average percentage error in viscosity (rMAPE), $\Delta\eta\,(\%)$, listed in Table IV, are determined from an equation of the type

$$\Delta\eta\,[\%] = \frac{100}{N}\sum\nolimits_i \left|1 - \frac{\eta_i^{calc}}{\eta_i^{\exp}}\right|. \tag{13}$$

Values for rMAPE, $\Delta\eta\,(\%)$, were calculated for the zero-shear viscosity model fits of the viscosity data. The viscosity–hole fraction equation given in (7) is found to represent the measured viscosity data of five species with mean percentage errors of 0.35%. The results are shown in Table IV. The expository procedure of viscosity prediction is given in Appendix B.

In an effort to elaborate the logarithmic viscosity-thermooccupancy correlation, in Fig. 7 $\ln(\eta_0)$ vs Y_h is plotted for the tested materials. As displayed in Fig. 7, (7) provides good linearization of

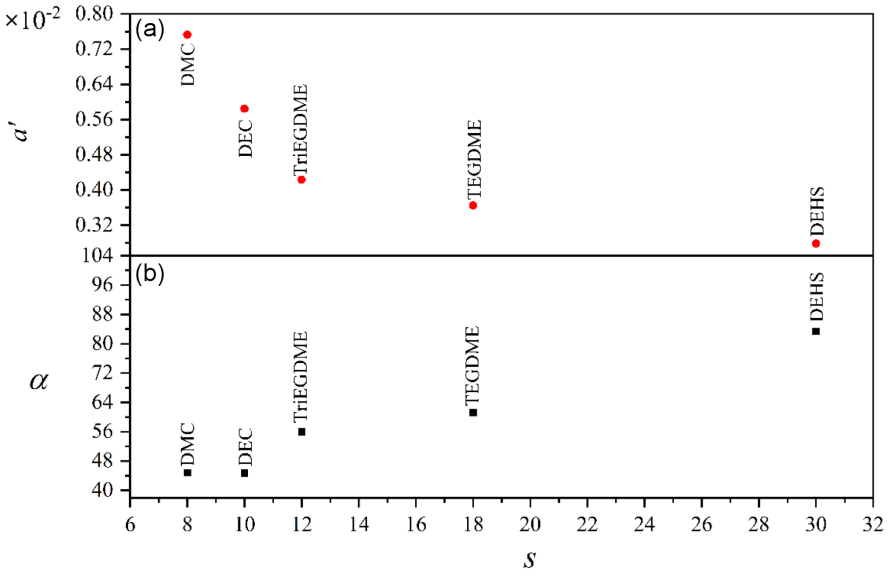

Fig. 8. Variation in a' and α with s at atmospheric pressure and 0°C for each sample in Table I.

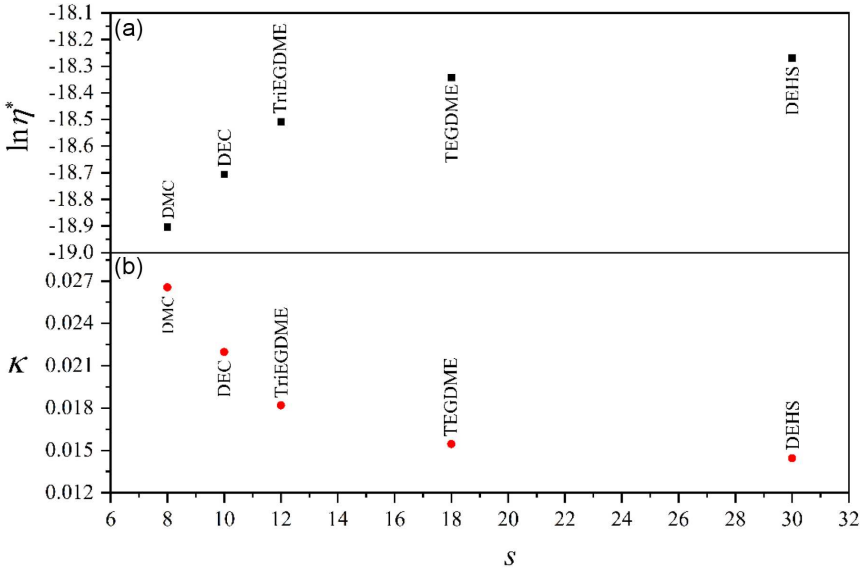

Fig. 9. Variation in $\ln(\eta^*)$ and κ with s at atmospheric pressure and 0°C for each sample from Table I.

$\ln(\eta_0)$ vs Y_h data. The lines correspond to the best approximation of the data set for each species. On the line, the pressure goes up from the lower to the upper part for each temperature, while regarding any fixed pressure data, temperature drops as it goes higher. In the lower part of the lines, where pressure drops and temperature rises, the lines converge, whereas at the upper part, they diverge. Going down the line, higher temperature and lower pressure increase the amount of hole fraction and result in the accumulation of molecules readily into the nano-voids. Conversely, going to a lower temperature and higher pressure, the decrease in free volume and hole fraction produces less transportation of molecules, specifically those with longer chain lengths and an increased number of CH_2 groups, since they occupy a larger free volume. In Fig. 7, at a given Y_h value, the viscosity of the samples are in the following order: DEHS > TEGDME > TriEGDME > DEC > DMC. The most inviscid material is DMC, with the lowest segment number.

The proportionality constant of the activation energy, a', listed in Table IV and illustrated in Fig. 8a, was found to decrease with segment number, s. The activation energy coefficient, a', is expected to have a similar tendency as α, the measure of activation energy. However, while comparing Fig. 8a to Fig. 8b, one can easily observe that they present the opposite trend because of the factor Φ, segment–segment interaction potential in (8). Concerning a', the order

of the magnitude is as follows: DEHS < TEGDME < TriEGDME < DEC < DMC. According to Table II, the sequence of the absolute value of Φ across the materials is TEGDME > TriEGDME > DEHS > DMC > DEC. This is caused by the fact that the introduction of polar ether groups produces stronger dipole–dipole interaction in glymes [2, 3]. Ultimately, the sequence of the a' value may differ from that of the value of α depending on the value of Φ, as expected.

The slopes of fitting lines in Fig. 7, yielding the values of α, are the measure of activation energy. The slope of the lines can give information on the viscous degree of the materials. From Table IV, we can say that the order of the materials concerning the measure of activation energy, α, is DEHS > TEGDME > TriEGDME > DMC > DEC. This points to the fact that the introduction of polar methylene groups enhances the viscosity except for DMC, which has a slightly higher α value than DEC. This inverse variation for dialkyl carbonates is seen in the internal pressure data for the same samples in the work of Comunas [3]. The contrary behavior concerning the α values in Table IV is illustrated in Fig. 8b in the form of the graph of α vs segment number s. It is visible that as the chain length of the species goes up, the materials exhibit larger slopes, α. The behavior of α is inverse to that of a' and of h and the slope of h in Fig. 4. In other words, the viscosity augments as the number of CH_2 groups increases.

Table IV shows that the transmission coefficient κ and $\ln(\eta^*)$, derived from (7) and (8) are inversely related to each other (see (8)). It can be seen from Table IV and Fig. 9 that κ decreases with chain length, whereas $\ln(\eta^*)$ increases with segment number across the materials. In other words, the one with a higher viscosity has a lower transmission coefficient, and vice versa. High temperature and low pressure give rise to the hole fraction, and the contribution to the viscosity from Y_h is diminished, as observed in (7) and (9). In this case, $\ln(\eta_0)$ would be equal to viscosity intercepts $\ln(\eta^*)$. The materials with higher viscosity have produced less free volume at elevated temperature and low-pressure states and ultimately have the more viscous effect (or viscosity intercepts $\ln(\eta^*)$). This hinders the molecules from moving into the holes and results in a reduction in the feasibility of the transmission with κ, values of which range from 0 to 1. According to Fig. 9, DMC has the lowest viscosity but the maximum transmission coefficient at the highest hole fraction due to the high temperature and low pressure.

Using (7), it is simple to obtain the differentiation of the logarithm of viscosity (viscoholibility). Figure 10 delineates a typical plot of viscoholibility divided by the structure-related parameter, $-\alpha$, in the linear equation vs hole fraction. The figure elucidates the viscosity alteration in accordance with the vacancy fraction function, h, at constant T as the fraction h shifts on the abscissa axis.

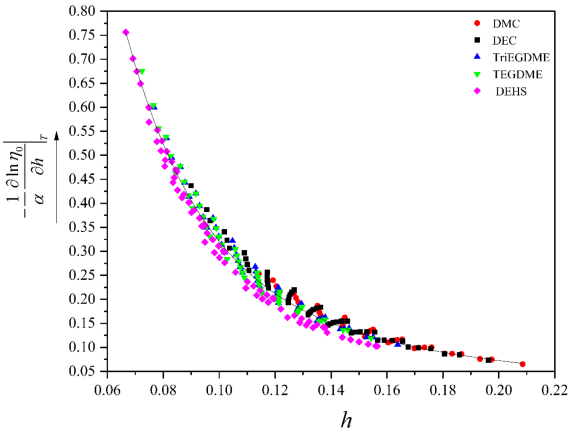

Fig. 10. Variation in $(-1/\alpha)(\partial \ln(\eta_0)/\partial h)\big|_T$ with h using (11) for each sample.

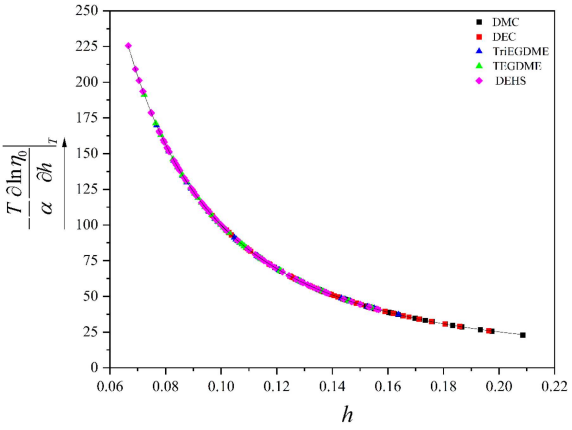

Fig. 11. Variation in $(-T/\alpha)(\partial \ln(\eta_0)/\partial h)\big|_T$ with h using (11) for each sample.

The full data are overlapped on the ordinate axis when multiplying the viscoholibility given in (11) by $-1/\alpha$, where α is the structure-related parameter specified in (8). The solid curve epitomized by

$$\frac{\partial \ln(\eta_0)}{\partial h}\Big|_T = -\alpha \left\{ 1.575 - 0.757 \left[1 - \mathrm{e}^{-(h+0.157)/0.175} \right] \right.$$

$$\left. -0.849 \left[1 - \mathrm{e}^{-(h+0.556)/0.0284} \right] \right\} \qquad (14)$$

stands for the exponential fit through the theoretical results. In Fig. 10, it is clearly seen that at the reduced values of h, the absolute value of the derivative function for logarithmic viscosity drastically changes to lower points. Specifically, the viscoholibility falls by a factor of four with a small negative curvature when the hole fraction is almost twofold. Along with this, the diminution of viscoholibility is systematically less and less pronounced and dwindles almost linearly with rising hole fraction. After a point $h \simeq 0.18$, we notice only a nominal change in the derivative function, and the $(-1/\alpha)(\partial \ln(\eta_0)/\partial h)\big|_T$ value scales down

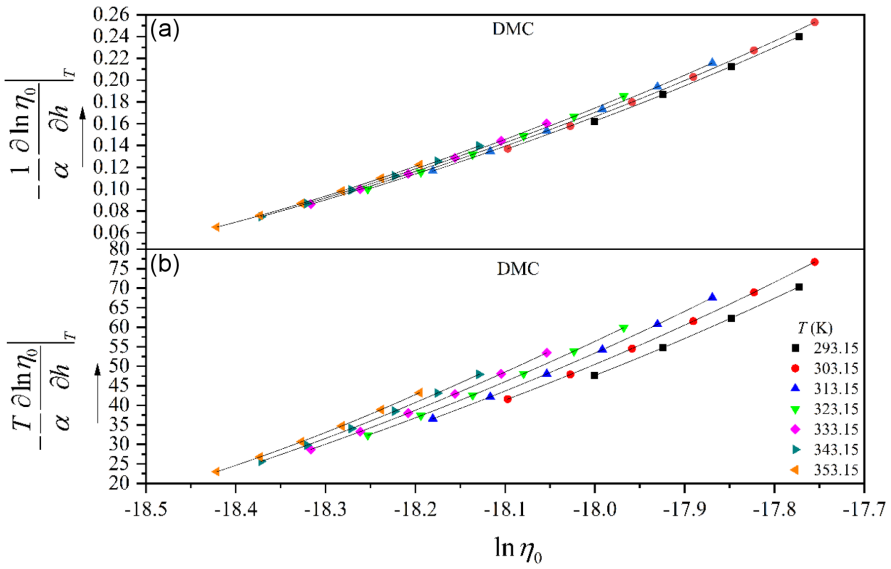

Fig. 12. Variation in (a) $(-1/\alpha)(\partial \ln(\eta_0)/\partial h)\big|_T$ and (b) $(-T/\alpha)(\partial \ln(\eta_0)/\partial h)\big|_T$ with $\ln(\eta_0)$ using (7) and (11) for DMC.

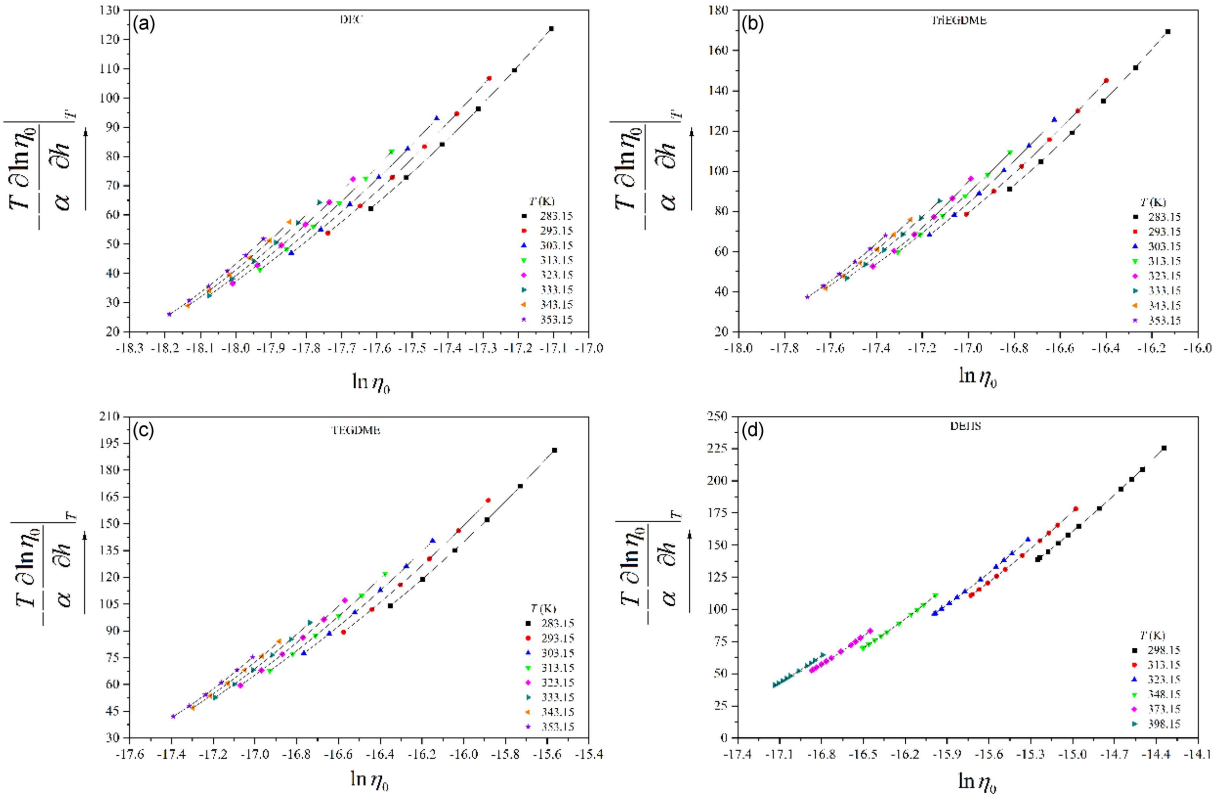

Fig. 13. Variations in $(-T/\alpha)(\partial \ln(\eta_0)/\partial h)\big|_T$ with $\ln(\eta_0)$ by means of (7) and (11), for (a) DECs, (b) TriEGDME, (c) TEGDME, (d) DEHS.

monotonically with h. It plateaus at a hole fraction of about $\simeq 0.031\alpha$ and remains nearly unchanged in the range where the hole fraction is in excess. The multiplication of viscoholibility on the vertical axis by temperature T results in a vanish of the scatter in Fig. 10 (see Fig. 11).

Graphical representation of $(-1/\alpha)(\partial \ln(\eta_0)/\partial h)\big|_T$ and $(-T/\alpha)(\partial \ln(\eta_0)/\partial h)\big|_T$ with respect to zero-shear viscosity is shown in Figs. 12 and 13. These functions increase in proportion to the logarithm of the zero-shear viscosity. At the lower parts, the curves converge

since the change in a small amount of viscosity as a function of hole fraction is not so different in terms of zero-shear viscosity values. In both mentioned figures, $\ln(\eta_0)$ increases as temperature decreases.

4. Conclusions

A pressure–volume–temperature (PVT) correlation with the predictive dynamic viscosity of dialkyl carbonates, two alkylene glycol dialkyl ethers, and a diester was probed by the using a zero-shear viscosity model. The equation bridges the Simha–Somcynsky equation of state via the nano-void fraction parameter. The outline of the present contribution is sketched as follows:

- The diester and polyeters (glymes) with longer chained structures and polar CH_2(methylene) groups or non-polar C_2H_4(ethylene) groups are denser and have increasing effects in the mean characteristic attractive interaction energy $\langle\varepsilon^*\rangle$ compared to short-chain carbonates, DACs. It is found that in glymes, the $\langle\varepsilon^*\rangle$ values are increasing due to the strong dipole–dipole interactions induced by the presence of ether groups. TEGDME (tetraglyme), the higher member of the polyether series, has higher $\langle\varepsilon^*\rangle$ values.
- The comparison between the published and theoretical values revealed by the earlier reported physically-based zero-shear viscosity correlation equation reports excellent consistency. The model incorporating the thermo-occupancy function, Y_h, verifies that the viscosity is inversely interrelated to the hole fraction. In general, the logarithmic viscosity of the individual materials exhibits a linear dependency on the thermo-occupancy function, Y_h, which is a function of T and h. The viscoholibility with a factor of $-1/\alpha$, the rate of change in dynamic viscosity of a sample over a computed hole fraction range, steps down with fraction h.
- Dialkyl carbonates with a decreased number of CH_2 groups, appear with the lower activation energy measure, α, which is the slope of the lines in the logarithm of viscosity against the Y_h plot. DEHS — the longer chained material with an increased number of CH_2 groups — has the higher α values. The results acquired for α are akin to ε^* since both of the parameters have inverse relevance to the distance between molecules.
- The computed hole fraction, h, values are higher but Y_h values are lower for dialkyl carbonates. Hereof, lower hole fraction values increase viscosity while reduced Y_h dwindles it. Consequently, longer chained samples with an increased number of polar groups have higher viscosity effects than samples with fewer carbon numbers, possessing fewer CH_2 groups.

Acknowledgments

This work did not receive any specific grant from funding organizations in the public, commercial, or non-profit sectors.

Appendix: Viscosity prediction procedure

Appendix A: Computing hole fraction (h) through Simha–Somcynsky equation of state (SS-EoS)

Hole fraction parameter (h) can be determined by the well-known Simha–Somcynsky equation of state (SS-EoS) of the form

$$\frac{\tilde{P}\tilde{V}}{\tilde{T}} = \frac{1}{1-\beta} + \frac{2y}{\tilde{T}} Q\,(AQ - B)\,, \tag{15}$$

$$\frac{s}{3c}\left[\frac{s-1}{s} + \frac{\ln(1-y)}{y}\right] - \frac{\beta - \frac{1}{3}}{1-\beta} - \frac{y}{6\tilde{T}} Q\,(2A - 3BQ) = 0, \tag{16}$$

where $Q = (y\tilde{V})^{-2}$ and $\beta = 2^{-1/6} y (y\tilde{V})^{-1/3}$, and A and B correspond to the constants 1.011 and 1.2045, respectively. The occupied (filled) site fraction, y, can be given in terms of hole fraction, h, as $y = 1-h$. The scaled parameters $\tilde{P}, \tilde{V}$, and $\tilde{T}$ are reduced by the characteristic parameters P^*, V^*, and T^* as $\tilde{P} = P/P^*$, $\tilde{V} = V/V^*$, and $\tilde{T} = T/T^*$. The characteristic scaling parameters P^*, V^*, and T^* are given as $q_z\varepsilon^*/(s\upsilon^*)$, $N_A\upsilon^*/m_0$, and $q_z\varepsilon^*/(ck)$, respectively.

The relation between the characteristic scaling parameters is

$$\frac{P^*V^*}{T^*} m_0 = \frac{c}{s} R. \tag{17}$$

Once the characteristic parametric quantities (P^*, V^*, T^*) are ascertained alongside the structural flexibility quantity, $3c/s$, and Lennard–Jones interaction quantities (υ^* and ε^*), outputs for $h = h(\tilde{P}, \tilde{T})$ can be yielded.

In order to evaluate the parameters P^*, V^*, T^* in the Mathematica program, it is necessary to have (15) in an employable format. With some adjustments, (15) takes the following form

$$0 = \tilde{T} - (1-\beta)\left(\tilde{P}\tilde{V} - 2yQ[AQ - B]\right). \tag{18}$$

To adapt the governing equations to the Mathematica code [36], (15) and (16) take the form

$$eos = T - (1-\beta)\Big(PV - 2yQ(AQ - B)\Big), \tag{19}$$

$$\text{eqlb} = (1/\text{cs})(\text{sratio} + \text{Log}[1-y]/y) - (\beta - 1/3)/(1-\beta) - [y/(6T)]Q(2B - 3AQ), \tag{20}$$

where P, V, and T refer to $\tilde{P}, \tilde{V}$ and $\tilde{T}$. The terms "cs" and "sratio" correspond to the ratios $3c/s$ and $(s-1)/s$ in (16), respectively. The function "Log" in the Mathematica program code corresponds to "ln" function in (16), which gives the natural logarithm of $(1-y)$ (logarithm to base e).

Each of the measured pressure–volume–temperature (P–V–T) data [2], respectively, in MPa, m^3/kg, and K units, is fitted to the model, namely (19) and (20). In order to have (19) with a solvable formatting, we need to reduce the unknown parameters and supply an initial adjustable value for c in (20). With the help of (20), y can be found in terms of V^* and T^* and inserted into (19). Thus, the latter becomes an equation with two unknown parameters, V^* and T^*.

Let us take diethyl carbonate (DEC) as an example and list the PVT data in the form below. To reduce data overflow, it is demonstrated only for a single temperature:

```
In [•] =   TPV exp =
{{283.15‘, 0.1‘, 0.0010140959334753068‘},
{283.15‘, 5.‘, 0.0010099899000101‘},
{283.15‘, 10.‘, 0.0010058338362502516‘},
{283.15‘, 15.‘, 0.001002004008016032‘},
{283.15‘, 20.‘, 0.00099830288509533 8‘},
{283.15‘, 25.‘, 0.000994826900119379‘},
{283.15‘, 30.‘, 0.00099137503717 6564‘},
{283.15‘, 35.‘, 0.0009880446596186147‘},
{283.15‘, 40.‘, 0.0009848335631278313‘},
{283.15‘, 45.‘, 0.0009817396426467701‘},
{283.15‘, 50.‘, 0.0009786651008025053‘},
{283.15‘, 55.‘, 0.0009758953840148336‘},
{283.15‘, 60.‘, 0.0009731413001167769‘}, ...
```

With N number of PVT data, (19) becomes N number of nonlinear equations with two unknown parameters, V^* and T^*. From simultaneous fitting, V^* and T^* will be computed by (19). The root of (20), y, is found by the Mathematica built-in function FindRoot that implements the Newton–Raphson method:

```
In [•] =   rooty =
FindRoot[eqlb == 0, {y, 0.999, 0.7, 0.9999}];
```

The output of the FindRoot command is stored in the variable "rooty." The arguments are the model, eqlb == 0, to be fitted, and the independent variable, y. The function FindRoot searches for a numerical root of eqlb == 0, starting from the point $y = 0.7$ between the points of 0.999 and 0.9999.

Reducing the unknowns in (20) allows (19) to be written as N number of equations with two unknown parameters (V^* and T^*), where each equation containing different temperature and pressure data. Then, the N number of the nonlinear system of equations with V^* and T^* denoted by VS and TS, can be illustrated as follows

$$\begin{aligned} eos_1 &= eos_1\,(VS, TS) = 0 \\ eos_2 &= eos_2\,(VS, TS) = 0 \\ eos_3 &= eos_3\,(VS, TS) = 0 \\ &\vdots \\ eos_N &= eos_N\,(VS, TS) = 0 \end{aligned}, \tag{21}$$

where eos is the abbreviated form of "equation of state." Here, (21) is a set of nonlinear transcendental equations with two unknowns, VS and TS. These equations can be solved using the Newton–Raphson method [36]. According to this method, it starts by giving appropriate initial values to the parameters, VS and TS. The following is an input for two initial guesses for $VS^{(0)}, TS^{(0)}$ and an arbitrary value given for c used in the Mathematica program:

```
In [•] =   VS = 0.9 × 10^-3; TS = 9000.; c = 1.03;
```

If the constituents of one iteration are denominated to be $VS^{(i)}, TS^{(i)}$, the Taylor expansion of the first expression in (21) near these constituents is written as (ignoring the second and upper terms)

$$\begin{aligned} eos_1\left(VS^{(i+1)}, TS^{(i+1)}\right) &\approx eos_1\left(VS^{(i)}, TS^{(i)}\right) \\ &+ \left.\frac{\partial eos_1}{\partial VS}\right|_{VS^{(i)}} \left(VS^{(i+1)} - VS^{(i)}\right) \\ &+ \left.\frac{\partial eos_1}{\partial TS}\right|_{TS^{(i)}} \left(TS^{(i+1)} - TS^{(i)}\right). \end{aligned} \tag{22}$$

In the same manner, the rest of the equations in (21) are obtained as

$$\begin{aligned} eos_2\left(VS^{(i+1)}, TS^{(i+1)}\right) &\approx eos_2\left(VS^{(i)}, TS^{(i)}\right) \\ &+ \left.\frac{\partial eos_2}{\partial VS}\right|_{VS^{(i)}} \left(VS^{(i+1)} - VS^{(i)}\right) \\ &+ \left.\frac{\partial eos_2}{\partial TS}\right|_{TS^{(i)}} \left(TS^{(i+1)} - TS^{(i)}\right) \\ &\vdots \\ eos_N\left(VS^{(i+1)}, TS^{(i+1)}\right) &\approx eos_N\left(VS^{(i)}, TS^{(i)}\right) \\ &+ \left.\frac{\partial eos_N}{\partial VS}\right|_{VS^{(i)}} \left(VS^{(i+1)} - VS^{(i)}\right) \\ &+ \left.\frac{\partial eos_N}{\partial TS}\right|_{TS^{(i)}} \left(TS^{(i+1)} - TS^{(i)}\right). \end{aligned} \tag{23}$$

Being the constituents of the vector $VS^{(i+1)}$ and $TS^{(i+1)}$, the following system of linear equations with two unknowns is provided

$$\begin{pmatrix} eos_1\left(VS^{(i+1)},TS^{(i+1)}\right) \\ eos_2\left(VS^{(i+1)},TS^{(i+1)}\right) \\ \vdots \\ eos_N\left(VS^{(i+1)},TS^{(i+1)}\right) \end{pmatrix} = \begin{pmatrix} eos_1\left(VS^{(i)},TS^{(i)}\right) \\ eos_2\left(VS^{(i)},TS^{(i)}\right) \\ \vdots \\ eos_N\left(VS^{(i)},TS^{(i)}\right) \end{pmatrix} + \begin{pmatrix} \frac{\partial eos_1}{\partial VS}\Big|_{VS^{(i)}} & \frac{\partial eos_1}{\partial TS}\Big|_{TS^{(i)}} \\ \frac{\partial eos_2}{\partial VS}\Big|_{VS^{(i)}} & \frac{\partial eos_2}{\partial TS}\Big|_{TS^{(i)}} \\ \vdots & \\ \frac{\partial eos_N}{\partial VS}\Big|_{VS^{(i)}} & \frac{\partial eos_N}{\partial TS}\Big|_{TS^{(i)}} \end{pmatrix} \begin{pmatrix} VS^{(i+1)}-VS^{(i)} \\ TS^{(i+1)}-TS^{(i)} \end{pmatrix}, \tag{24}$$

where $VS^{(i+1)}$, $TS^{(i+1)}$ and $VS^{(i)}$, $TS^{(i)}$ are the root estimates in the $(i+1)$-th and i-th iterations, respectively.

Besides entailing an initial guess, the Newton–Raphson method necessitates determining the derivatives of the functions, $eos_1, eos_2, \ldots, eos_N$. In the following Mathematica code the derivative of the governing equation in the linear system of equations "eos" with respect to the parameters $VS^{(i)}, TS^{(i)}$ in (24) is taken and solved:

```
In [•] =   eosVS = D[eos, VS];
In [•] =   eosTS = D[eos, TS];
```

and "D" gives the partial derivative $\partial(eos)/\partial(VS)$.

We assume that the values of $VS^{(i+1)}$ and $TS^{(i+1)}$ in (24) are close to the root of the equations. Thus, by setting the left-hand side of (24) to zero, a coveted quantity for the functions $eos_1, eos_2, \ldots, eos_N$, (24) can be recorded as

$$\underbrace{\begin{pmatrix} \frac{\partial eos_1}{\partial VS}\Big|_{VS^{(i)}} & \frac{\partial eos_1}{\partial TS}\Big|_{TS^{(i)}} \\ \frac{\partial eos_2}{\partial VS}\Big|_{VS^{(i)}} & \frac{\partial eos_2}{\partial TS}\Big|_{TS^{(i)}} \\ \vdots & \\ \frac{\partial eos_N}{\partial VS}\Big|_{VS^{(i)}} & \frac{\partial eos_N}{\partial TS}\Big|_{TS^{(i)}} \end{pmatrix}}_{A} \underbrace{\begin{pmatrix} VS^{(i+1)}-VS^{(i)} \\ TS^{(i+1)}-TS^{(i)} \end{pmatrix}}_{\Delta S} = \underbrace{\begin{pmatrix} -eos_1\left(VS^{(i)},TS^{(i)}\right) \\ -eos_2\left(VS^{(i)},TS^{(i)}\right) \\ \vdots \\ -eos_N\left(VS^{(i)},TS^{(i)}\right) \end{pmatrix}}_{EOS}. \tag{25}$$

By setting $A_{ab} = \frac{\partial eos_a}{\partial S_b}\Big|_{S^{(i)}}$, (25) can be compactly rewritten in matrix format as

$$A\,\Delta S = EOS, \tag{26}$$

where A is an $N \times 2$ matrix. Both ΔS and EOS are 1-dimensional matrices. While ΔS is a two-dimensional vector, EOS is an N-dimensional vector of N components. The former has the components of $(VS^{(i+1)} - VS^{(i)})$ and $(TS^{(i+1)} - TS^{(i)})$, whereas the latter has $eos_1\left(VS^{(i)},TS^{(i)}\right)$, $eos_2\left(VS^{(i)},TS^{(i)}\right)$, …, $eos_N(VS^{(i)},TS^{(i)})$.

From (26), the searched ΔS can be computed. Due to the fact that A is not a square matrix, the inverse of matrix A can be found by the pseudo-inverse matrix technique

$$\Delta S = \text{PseudoInverse}\,[A]\,EOS \Rightarrow$$
$$\Rightarrow S^{(i+1)} = S^{(1)} + \Delta S, \tag{27}$$

where S denotes either VS or TS. Hence we can write the following

$$VS^{(i+1)} = VS^{(i)} + \Delta VS^{(i)},$$
$$TS^{(i+1)} = TS^{(i)} + \Delta TS^{(i)}. \tag{28}$$

The argument by which we gain the differences between the values of VS and TS for two sequential iterations in the Mathematica code is:

```
In [•] = δPVT = PseudoInverse[eosdiff].eosvalue;
```

In order to find the roots (VS and TS) the iteration is done until reaching the specific criteria for ΔS, which are $\Delta VS < 10^{-8}$ and $\Delta TS < 0.1$. Function δPVT summarizes this criteria:

```
In [•] =   δPVT
Out [•] =   {−1.24388 × 10^−9, 0.050156}
```

The Mathematica code by which we perform these criteria is:

```
In [•] =   If[Abs[δVT][[1]]>10^−8||Abs[δVT][[2]]>0.1,
Goto[start]];
```

For $i = 0$, the optimized initial values of $VS^{(0)}$ and $TS^{(0)}$, together with the arbitrary value given for c, are:

```
In [•] =   VS = 0.9 × 10^−3; TS = 9000.; c = 1.03;
```

The following is a function evaluating the roots based on the two initial guesses for $\text{VS}^{(0)}$ and $\text{TS}^{(0)}$:

```
In [•] =   {VS, TS} = {VS, TS} − ΔPVT;
```

where {VS, TS} is the function to extract the data:

```
In [•] =   {VS, TS}
Out [•] =   {0.000939452, 10316.7}
```

With the known V^* and T^*, P^* can be directly generated from (17). The results for a theoretical specific volume V, which appeared as Ve in the Mathematica program, are extracted from the

function below:

In [•] = rooty = FindRoot[{eos == 0, eqlb == 0},
{y, 0.999, 0.7, 0.9999], }
{Ve, Vexp, 0.8×10^{-3}, 1.4×10^{-3}}];

Here, as usual, we are storing the output of the "FindRoot" command in the variable "rooty." The function "FindRoot" searches for a numerical solution to the simultaneous equations *eos*==0, eqlb==0, starting from the point $y = 0.7$ between the points 0.999 and 0.9999, while for Ve, i.e., Ve = Vexp, from a starting point between 0.8×10^{-3} and 1.4×10^{-3}.

The input and the last output of the function "rooty" appearing in the Mathematica code are:

In [•] = rooty

Out [•] = {y → 0.843389, Ve → 0.0010356}

These output results indicate the last data of the set. Some of the computed values for y, h, and Ve are respectively listed as follows:

In [•] = ylist

Out [•] = {...,
0.8141393468196124‘, 0.8180487037355209‘,
0.8218272488133972‘, 0.8254139989885313‘,
0.828826946879309‘, 0.8320815829698343‘,
0.8351913497331729‘, 0.8381679956961274‘,
0.8410218550107478‘, 0.8437620707843877‘,
0.8463967753395603‘, 0.8489332371574052‘,
0.8513779816119692‘, 0.8537463389075111‘,
0.8579472927519048‘, 0.8119971640928816‘,
0.8158326090000432‘, 0.8194747452320005‘,
0.822941609773851‘, 0.8262487442219549‘,
0.8294096454511466‘, 0.8324361174298367‘,
0.8353385493172075‘, 0.8381261379057054‘,
0.8408070673435072‘, 0.8433886557359095‘}

In [•] = TPhlist

Out [•] = {...,
{353.15‘, 0.1‘, 0.19625366109248887‘},
{353.15‘, 5.‘, 0.1920527072480952‘},
{353.15‘, 10.‘, 0.18800283590711842‘},
{353.15‘, 15.‘, 0.18416739099995683‘},
{353.15‘, 20.‘, 0.18052525476799952‘},
{353.15‘, 25.‘, 0.177058390226149‘},
{353.15‘, 30.‘, 0.17375125577804507‘},
{353.15‘, 35.‘, 0.1705903545488534‘},
{353.15‘, 40.‘, 0.1675638825701633‘},
{353.15‘, 45.‘, 0.16466145068279248‘},
{353.15‘, 50.‘, 0.16187386209429455‘},
{353.15‘, 55.‘, 0.1591929326564928‘},
{353.15‘, 60.‘, 0.1566113442640905‘}}

(In the above Mathematica code, the third term in the curly bracket indicates the hole fraction.)

In [•] = PVTlst

Out [•] = {...,
{353.15, 0.1, 0.00110348}, {353.15, 5., 0.00109615},
{353.15, 10., 0.00108911}, {353.15, 15., 0.00108248},
{353.15, 20., 0.00107621}, {353.15, 25., 0.00107027},
{353.15, 30., 0.00106462}, {353.15, 35., 0.00105924},
{353.15, 40., 0.0010541}, {353.15, 45., 0.00104918},
{353.15, 50., 0.00104447}, {353.15, 55., 0.00103995},
{353.15, 60., 0.0010356}}

(The second term in the curly brackets represents the theoretical volume.)

In the process of altering c with the aim of estimating the best-fit parameters, P^*, V^*, T^* together with υ^* and ε^*, the optimum values are obtained at the least relative mean absolute percentage error, (rMAPE):

Out [•] = s = 8., c = 1.06%, err = 0.0383687,
V^* = 0.000939452, T^* = 10316.7, P^* = 819.271,
vs = 0.000013871968229837989‘,
ϵs = 133.36189186169878‘,
mo = 0.014766024999999999‘,
Max%Error = 0.37956267087386214‘

Here, vs and ϵs denote υ^* and ε^*, respectively.

We have evaluated the roots of (19), y, so h can be generated from (20). The generation of h can support the experimental determinations of dynamic viscosity (η). Dynamic viscosity can be obtained from the procedure described in the upcoming Appendix B.

Appendix B: Non-linear fit data to zero-shear viscosity (dynamic viscosity) model

The previously published zero-shear viscosity model requires lubricant hole fraction extracted from PVT measurements through SS-EoS. Once the h values are obtained, the Newtonian viscosity can be predicted through the viscosity model using the published data [3, 12]. The raw viscosity inputs for diethyl carbonate (DEC) (in the unit [Pa s]) together with the given temperature and pressure are:

In [•] = Texη = {283.15, 293.15‘, 303.15‘, 313.15‘,
323.15‘, 333.15‘, 343.15‘, 353.15‘};
Pexη =
{{0.1‘, 20.‘, 40.‘, 60.‘, 80.‘, 100.‘},
{0.1‘, 20.‘, 40.‘, 60.‘, 80.‘, 100.‘},
{0.1‘, 20.‘, 40.‘, 60.‘, 80.‘, 100.‘},
{0.1‘, 20.‘, 40.‘, 60.‘, 80.‘, 100.‘},
{0.1‘, 20.‘, 40.‘, 60.‘, 80.‘, 100.‘},
{0.1‘, 20.‘, 40.‘, 60.‘, 80.‘, 100.‘},
{0.1‘, 20.‘, 40.‘, 60.‘, 80.‘, 100.‘},
{0.1‘, 20.‘, 40.‘, 60.‘, 80.‘, 100.‘}};

η0List =
{{0.935, 1.130, 1.315, 1.500, 1.705, 1.925},
{0.810, 0.965, 1.115, 1.260, 1.425, 1.605},
{0.710, 0.840, 0.975, 1.110, 1.250, 1.395},
{0.625, 0.735, 0.860, 0.990, 1.130, 1.270},
{0.560, 0.665, 0.780, 0.900, 1.015, 1.125},
{0.495, 0.585, 0.685, 0.790, 0.895, 1.005},
{0.445, 0.540, 0.625, 0.720, 0.825, 0.935},
{0.405, 0.485, 0.560, 0.640, 0.730, 0.825}} $\times 10^{-3}$;

In Mathematica code, Texη, Pexη, and η0List signify the experimental temperature, pressure, and viscosity data, respectively.

Dynamic viscosity is given a set of 48 data points with 8 subsets having 6 data each. In the viscosity data group, each subgroup corresponds to the each temperature given in the set of Texη. In each viscosity subgroup, each datum corresponds to each pressure given in each Pexη subgroup.

The zero-shear viscosity model has the form

$$\ln(\eta_0) = \ln(\eta^*) + \alpha Y_h, \tag{29}$$

where Y_h is given as

$$Y_h = (1-h)/(hT). \tag{30}$$

So the data in the set of η0List needs to be converted to logarithmic form:

In [•] = ηlog

Out [•] =
{{−17.4745, −17.39, −17.3341, −17.2906,
−17.2444, −17.1999}, {−17.6121, −17.5442,
−17.4969, −17.4637, −17.4231, −17.3812},
{−17.7355, −17.6772, −17.627, −17.5875,
−17.5519, −17.5196}, {−17.8524, −17.803,
−17.7468, −17.6974, −17.6492, −17.6104},
{−17.9494, −17.8935, −17.837, −17.7868,
−17.7516, −17.7274}, {−18.0578, −18.0103,
−17.958, −17.9099, −17.8713, −17.8349},
{−18.1473, −18.0774, −18.0393, −17.9942,
−17.9455, −17.9007}, {−18.2226, −18.1703,
−18.1375, −18.1023, −18.0596, −18.0186}},

where ηlog represents the linearized data.

In (30), the hole fraction h is computed from SS theory described in Sect. 2. Here, the h values are extracted for the given temperature and pressure of viscosity in the code below:

In [•] = rooty = FindRoot[{eos == 0, eqlb == 0},
{y, 0.99, 0.6, 0.99999}, Ve, 1.1×10^{-3}, 0.8×10^{-3},
1.7×10^{-3}}]
Out [•] = {y → 0.861137, Ve → 0.00100588}

These output results for y and Ve are the last values of the "ylst" and "Velst" data, respectively. The lists for "ylst" and "Velst" represent the occupied site fraction and specific volume findings:

In [•] = ylst

Out [•] =
{{0.873216, 0.882771, 0.890997, 0.898159,
0.904475, 0.910104}, {0.863757, 0.874054,
0.882873, 0.890525, 0.897255, 0.903241},
{0.854143, 0.865223, 0.874661, 0.882818,
0.889974, 0.896325}, {0.844374, 0.856281,
0.866365, 0.875045, 0.882637, 0.88936},
{0.834452, 0.847233, 0.85799, 0.867211,
0.875251, 0.882355}, {0.824374, 0.83808,
0.849541, 0.85932, 0.86782, 0.875312},
{0.814139, 0.828827, 0.841022, 0.851378,
0.860349, 0.868238}, {0.803746, 0.819475,
0.832436, 0.843389, 0.852844, 0.861137}}
In [•] = Velst

Out [•] =
{{0.00101451, 0.000998757, 0.000985156,
0.000973252, 0.000962678, 0.000953175},
{0.00102577, 0.00100876, 0.000994184,
0.000981499, 0.000970283, 0.00096024},
{0.00103748, 0.0010191, 0.00100348,
0.000989962, 0.000978069, 0.000967461},
{0.00104965, 0.00102978, 0.00101304,
0.000998644, 0.000986037, 0.000974837},
{0.0010623, 0.00104082, 0.00102287,
0.00100755, 0.000994188, 0.000982367},
{0.00107547, 0.00105223, 0.00103299,
0.00101667, 0.00100252, 0.000990051},
{0.00108919, 0.00106402, 0.0010434,
0.00102602, 0.00101104, 0.000997889},
{0.00110348, 0.00107621, 0.0010541,
0.0010356, 0.00101974, 0.00100588}}

The following output is for the hole fraction parameter extracted from the occupied site fraction list:

In [•] = 1 − ylst

Out [•] =
{{0.126784, 0.117229, 0.109003, 0.101841,
0.0955246, 0.0898956}, {0.136243, 0.125946,
0.117127, 0.109475, 0.102745, 0.0967587},
{0.145857, 0.134777, 0.125339, 0.117182,
0.110026, 0.103675}, {0.155626, 0.143719,
0.133635, 0.124955, 0.117363, 0.11064},
{0.165548, 0.152767, 0.14201, 0.132789,
0.124749, 0.117645}, {0.175626, 0.16192,
0.150459, 0.14068, 0.13218, 0.124688},
{0.185861, 0.171173, 0.158978, 0.148622,
0.139651, 0.131762}, {0.196254, 0.180525,
0.167564, 0.156611, 0.147156, 0.138863}}

where "1-ylst" and "ylst" denote the list of h and y values for each temperature and pressure, respectively.

A template for the linearized model of the viscosity expression for (29) in the Mathematica code program is defined as:

$$\text{In}[\bullet] = \quad \text{model} = a_0 + a_1 \text{Yh}$$

where "model" is the function to extract the theoretical viscosity data:

$$\text{In}[\bullet] = \quad \text{model}$$

$$\text{Out}[\bullet] = \quad a_0 + (y\eta\, a_1)/(T\eta(1. - y\eta))$$

where a_0 and a_1 are the model parameters and are referred to as $\ln(\eta^*)$ and α in (29), respectively. The occupied site function is $y\eta = 1 - h$.

Fitting the experimental ηlog and h values to (29), 48 equations are built with two unknowns: a_0 and a_1. In order to solve these equations (to find the two parameters, a_0 and a_1), the following NonlinearModelFit command in Mathematica implementing the Newton–Raphson method is run:

$$\text{In}[\bullet] = \quad \text{ft} = \text{NonlinearModelFit}[\log\eta y T, \text{model}, \{a_0, a_1\}, \{y\eta, T\eta\}]$$

Here, the variable "ft" is used to keep the model Mathematica constitutes as a product of the fit. Of the arguments, "logηyT" is a list of viscosity, occupied site fraction, and temperature data, "model" is the function to be fitted, {a_0,a_1} is a list of the parameters to change, and {yη,Tη}] are the independent variables, occupied site fraction and temperature.

The parameters are stored in the function $\text{ft}_{[[1,2]]}$:

$$\text{In}[\bullet] = \quad \text{ft}_{[[1,2]]}$$

$$\text{Out}[\bullet] = \quad \{a_0 \to -18.705817075032986`, a_1 \to 44.69862360250618`\}$$

The predicted function for the viscosity expression is:

$$\text{In}[\bullet] = \quad \text{Log}\eta = -18.7058 + (44.6986 y\eta)/(T\eta(1. - y\eta))$$

By substituting the parameters back into the expression (29) together with the computed Yh values, the theoretical dynamic viscosity data are created. The Mathematica function for producing theoretical viscosity values is ηlogFitValue:

$$\text{In}[\bullet] = \quad \eta\text{logFitValue} = \text{Flatten}[\text{model}/.\text{ft}_{[[1,2]]}/.\{y\eta \to \text{ylst}, T\eta \to \text{Tden}\}]$$

The equation above tells us that the values of the parameters a_0 and a_1 stored in the function $\text{ft}_{[[1,2]]}$, the occupied site fraction yη, and temperature values Tden are fitted to the model. In the following, there are the outputs of the fit:

$$\text{In}[\bullet] = \quad \eta\text{logFitValue}$$

$$\text{Out}[\bullet] =$$
$$\{-17.6186, -17.5171, -17.4154, -17.3136, -17.2111, -17.1076, -17.7391, -17.6476, -17.5565, -17.4655, -17.3743, -17.2824, -17.8424, -17.7593, -17.6769, -17.595, -17.5132, -17.4311, -17.9314, -17.8554, -17.7804, -17.7062, -17.6323, -17.5584, -18.0086, -17.9387, -17.8701, -17.8025, -17.7353, -17.6684, -18.076, -18.0114, -17.9482, -17.8863, -17.8249, -17.7639, -18.1352, -18.0751, -18.0167, -17.9596, -17.9033, -17.8475, -18.1875, -18.1313, -18.077, -18.0242, -17.9723, -17.9209\}$$

The variable organized for the Y_h function appearing in (29) and its values in certain temperatures and pressures are, respectively:

$$\text{In}[\bullet] =$$
$$\text{YhValue} = \text{Flatten}[\text{Yh}/.\{y\eta \to \text{ylst}, T\eta \to \text{Tden}\}]$$

$$\text{Out}[\bullet] =$$
$$\{0.0243244, 0.0265949, 0.0288682, 0.0311467, 0.0334399, 0.0357549, 0.0216266, 0.0236736, 0.025713, 0.0277485, 0.0297897, 0.0318437, 0.0193173, 0.0211765, 0.0230195, 0.0248515, 0.0266823, 0.0285188, 0.0173261, 0.0190261, 0.0207028, 0.0223627, 0.0240159, 0.0256693, 0.0155981, 0.017162, 0.0186965, 0.0202096, 0.0217115, 0.0232094, 0.0140895, 0.0155363, 0.0169483, 0.0183351, 0.0197071, 0.0210717, 0.0127652, 0.0141106, 0.0154165, 0.0166938, 0.0179535, 0.0192028, 0.0115969, 0.012854, 0.0140673, 0.0152491, 0.0164109, 0.0175601\}$$

The reliability of the model is checked on rMAPE and coded as below. The variable "errinlogη" stores the rMAPE results, and $\eta\text{logFlat}_{[[3]]}$ is the function that signifies theoretical viscosity data. The statistics done on the parameter for this regression suggest a reasonable fit:

$$\text{In}[\bullet] = \quad \text{errinlog}\eta = 100(\eta\text{logFitValue} - \eta\text{logFlat}_{[[3]]})/\eta\text{logFlat}_{[[3]]};$$
$$\text{meanerr} = \text{Mean}[\text{Flatten}[\text{Abs}[\text{errinlog}\eta]]]$$

$$\text{Out}[\bullet] = \%\text{Error} =$$
$$\{0.824417, 0.730934, 0.469471, 0.133247, -0.193279, -0.536676, 0.721249, 0.589717, 0.3406, 0.0105538, -0.280167, -0.568163, 0.602273, 0.464355, 0.282752, 0.0426175, -0.220622, -0.505335, 0.442264, 0.294256, 0.189642, 0.0496961, -0.095517, -0.295125, 0.329998, 0.252628, 0.185505, 0.0879191, -0.0917127, -0.332908, 0.101009, 0.00570812, -0.0541786, -0.132184, -0.259588, -0.397717, -0.0665901, -0.0127551, -0.125205, -0.192123, -0.235159, -0.297469, -0.192869, -0.214727, -0.333149, -0.431369, -0.483377, -0.542175\}$$

The mean error organized into the Mathematica function is:

In [•] = meanerr = Mean[Flatten[Abs[errinlogη]]]

Out [•] = 0.296687

The theoretical viscosity results deviate from the literature by nearly 0.3%.

To justify the performance of the model, another regression error metric, the R-squared of the model, R^2, is calculated as shown in the code below:

In [•] = Print["R^2 = ", ft["RSquared"]]

Out [•] = $R^2 = 0.999987$

This means that the thermooccupancy function, Y_h, accounts for 99.9% of the variation in the viscosity.

References

[1] Y. Zhou, J. Wu, E.W. Lemmon, *J. Phys. Chem. Ref. Data* **40**, 043106-1 (2011).

[2] A. Baylaucq, M.J.P. Comunas, C. Boned, A. Allal, J. Fernandez, *Fluid Phase Equilib.* **199**, 249 (2002).

[3] M. J. P. Comunas, A. Baylaucq, C. Boned, J. Fernandez, *Int. J. Thermophys.* **22**, 749 (2001).

[4] X. Esteve, A. Conesa, A. Coronas, *J. Chem. Eng. Data* **48**, 392 (2003).

[5] A. Rodriguez, J. Canosa, A. Dominguez, J. Tojo, *J. Chem. Eng. Data* **48**, 146 (2003).

[6] K. Shukla, V.C. Srivastava, *Rsc. Adv.* **6**, 32624 (2016).

[7] A.B. Pereiro, A. Rodriguez, J. Canosa, J. Tojo, *J. Chem. Eng. Data* **49**, 1392 (2004).

[8] A.O.G. Abdalla, D. Liu, *Rev. Energies* **11**, 2 (2018).

[9] S. Huang, B. Yan, S. Wang, X. Ma, *Chem. Soc. Rev.* **44**, 3079 (2015).

[10] W. Song, H. Zhang, Z. Yang, J. Wang, Z. Yue, J. Yu, *Z. Phys. Chem.* 1 (2017).

[11] F. Chen, Z. Yang, Z. Chen, J. Hu, C. Chen, J. Cai, *J. Mol. Liq.* **209**, 683 (2015)

[12] X. Paredes, O. Fandino, A.S. Pensado, M.J.P. Comunas, J. Fernandez, *J. Chem. Thermodyn.* **44**, 38 (2012).

[13] W. Hirst, A.J. Moore, *Proc. R. Soc. Lond. A* **365**: 537 (1979).

[14] S. Bair, *Tribol. Lett.* **22**, 197 (2006).

[15] S. Boyde, *Esters from: Synthetics, Mineral Oils, and Bio-Based Lubricants, Chemistry and Technology*, Third Edition, CRC Press, London 2020.

[16] P. Vergne, *High Temp.-High Press.* **22**, 613 (1990).

[17] B. Guignon, C. Aparicio, P.D. Sanz, *J. Chem. Eng. Data* **55**, 3017 (2010).

[18] P. Vergne, *Metrologia* **30**, 669 (1994).

[19] C.L. Giusca, I. Severn, J. Greenwood, *J. Phys. Conf. Ser.* **121**, 1 (2008).

[20] S. Yadav, M. Singh, O. Prakash, A.K. Bandyopadhyay, V.R. Singh, *Int. J. Acoust. Vib.* **13**, 125 (2008).

[21] S.K. Mylona, M.J. Assael, K.D. Antoniadis, S.K. Polymatidou, L. Karagiannidis, *J. Chem. Eng. Data* **58**, 2805 (2013).

[22] R.J. Sadinski, C.H. Hager, Jr., W.M. Hannon, *J. Tribol.* **145**, 011601-1 (2023).

[23] A. Carlisle, L. Haber, C. Olsen, A. Parker, J. Patterson, A. Pecquet, J. Reichard, *Toxicity Review For Di(2-Ethylhexyl) Sebacate (DEHS)/Dioctyl Sebacate (DOS)*, Cincinnati (OH) 2019.

[24] F. Sahin-Dinc, C. Schaschke, U. Yahsi, *Int. J. Oil, Gas Coal Technol.* **30 (2)**, 209 (2022).

[25] F. Sahin-Dinc, *Acta Phys. Pol. A* **141**, 535 (2022).

[26] T.S. Ree, T. Ree, H. Eyring, *Proc. Natl. Acad, Sci. USA* **48**, 501 (1962).

[27] T.S. Ree, T. Ree, H. Eyring, *J. Phys. Chem.* **68**, 3262 (1964).

[28] U. Yahsi, *J. Poly. Sci. Pol. Phys.* **37**, 879 (1999).

[29] U. Yahsi, F. Sahin, *Rheol. Acta* **43**, 159 (2004).

[30] S. Glasstone, K.L. Laidler, H. Eyring, *Theory of Rate Processes*, McGraw-Hill Book Company, New York 1941.

[31] T.S. Ree, H. Eyring, T. Ree, *Proc. Natl. Acad. Sci. USA* **51**, 344 (1964).

[32] F.S. Dinc, T. Sedlacek, C. Tav, U. Yahsi, *J. Appl. Polym. Sci.* **131**, 40540 (2014).

[33] F. Sahin-Dinc, A. Sorrentino, C. Tav, U. Yahsi, *Int. J. Thermophys.* **36**, 3239 (2015).

[34] F. Sahin-Dinc, *Inter. Polym. Process.* **30**, 585 (2015).

[35] F. Sahin-Dinc, U. Yahsi, T. Sedlacek, *Adv. Polym. Technol.* **2019**, 1 (2019).

[36] Wolfram Research Inc., Mathematica, ver. 10.0, Champaign (IL) 2014.

[37] D.R. Caudwell, J.P.M. Trusler, V. Vesovic, W.A. Wakeham, *J. Chem. Eng. Data* **54**, 359 (2009).

[38] D.R. Caudwell, J.P.M. Trusler, V. Vesovic, W.A. Wakeham, *Int. J. Thermophys.* **25**, 1339 (2004).